A case study of South Australia's severe thunderstorm and tornado outbreak

Dragana Zovko-Rajak, Kevin Tory and Jeffrey Kepert, Bureau of Meteorology & Bushfire and Natural Hazards CRC.

Introduction

On September 28, 2016 one of the most significant thunderstorm outbreaks recorded in South Australia impacted central and eastern parts of the state. Multiple supercell thunderstorms were embedded in a Quasi-Linear Convective System (QLCS, Weisman & Trapp 2003) aligned with a strong cold front that was associated with an intense low-pressure system. The storms produced at least seven tornadoes, destructive wind gusts, large hail and intense rainfall. Transmission lines were brought down in four different locations, which contributed to a state-wide power outage.

Accurate prediction and understanding of tornadoes and other hazards associated with severe thunderstorms is very important, for timely preparation and announcement of warnings. By conducting high-resolution simulations, this study aims to offer a better understanding of the meteorology of the South Australian thunderstorm and tornado outbreak. It also contributes to improving knowledge of how to best predict similar severe weather events, which in turn enables better risk management and preparedness for such events. Updraft helicity (Kain et al. 2008), a severe storm surrogate that indicates the potential for updraft rotation in simulated storms, is used to investigate the ability of the model to predict supercell and tornado likelihood.

Numerical model description and set up

Here, a case study of the September 28, 2016 event is conducted using version 10.6 of the UK Met Office Unified Model (UM), the atmospheric component of the Australian Community Climate and Earth-System Simulator (ACCESS) (Puri et al. 2013). The model consists of a global model run (17 km horizontal grid spacing) that is nested down to grid spacing of 4.0 km, 1.5 km and 400 m (Fig. **Error! Reference source not found.**), with the inner domain size chosen to capture the area where seven tornadoes were reported. Each domain has 80 vertical levels and the model top for the nested domains is 38.5 km.

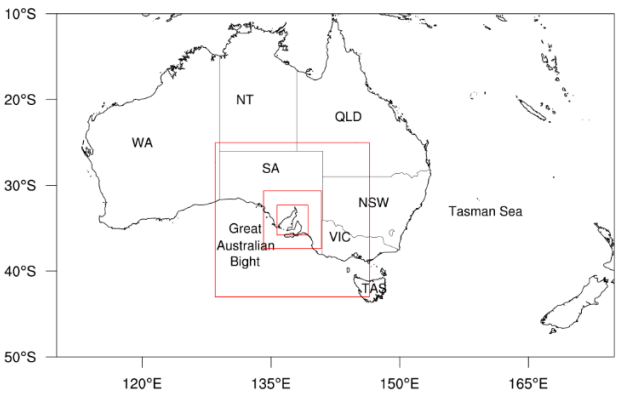

Figure 1: Outline of model domains, with the larger domain having horizontal grid spacing of 4 km, and the smaller domains have horizontal grid spacing of 1.5 km and 400 m.

In addition to the described deterministic simulations, convective-scale ensemble simulations of the same event were conducted to learn about the predictability of this event. For these simulations, version 11.1 of the UM ensemble nesting suite is used and consists of the Met Office global ensemble model (MOGREPS-G; Bowler et al. 2008) as a driving model, with a horizontal grid spacing of ~ 33 km, which is similarly nested down to 4 km, 1.5 km and 400 m regional domains.

The ensemble consists of 6 simulations (1 control + 5 perturbed) initialised at 1200 UTC 27 September 2016 (+ 9.5 hours for local time) and ran for 24 hours, with initial and boundary conditions for each member provided by the corresponding MOGREPS-G member. Like the deterministic model, all simulations use the RA1M science configuration and all domains have 80 vertical levels with the model top for nested domains of 38.5 km.All simulations use the Regional Atmosphere Mid-latitude first release (hereafter RA1M) science configuration (Bush et al. 2019), to assess model performance over the South Australia domain, and simulation results are compared to radar imagery. All simulations were initialised at 1500 UTC 27 September 2016 (+ 9.5 hours local time) and ran for 48 hours.

Simulation results

a) Deterministic simulations

To investigate how well the model represents severe thunderstorms, observed radar reflectivity (Fig. 2, left) is compared to simulated reflectivity (Fig. 2, right) from the 1.5 km model at 0600 UTC 28 September 2016. Figure 2a shows the line of thunderstorms that were associated with large hail and several reported tornadoes (Bureau of Meteorology 2016), and the overall timing and location of severe thunderstorms is captured well by the model (Fig. 2b). Individual supercells are not depicted by the model as grid lengths on order of 1 km are not able to fully resolve supercell or tornado-like signatures (e.g., Bryan, Wyngaard & Fritsch 2003; Hanley, Barrett & Lean 2016).

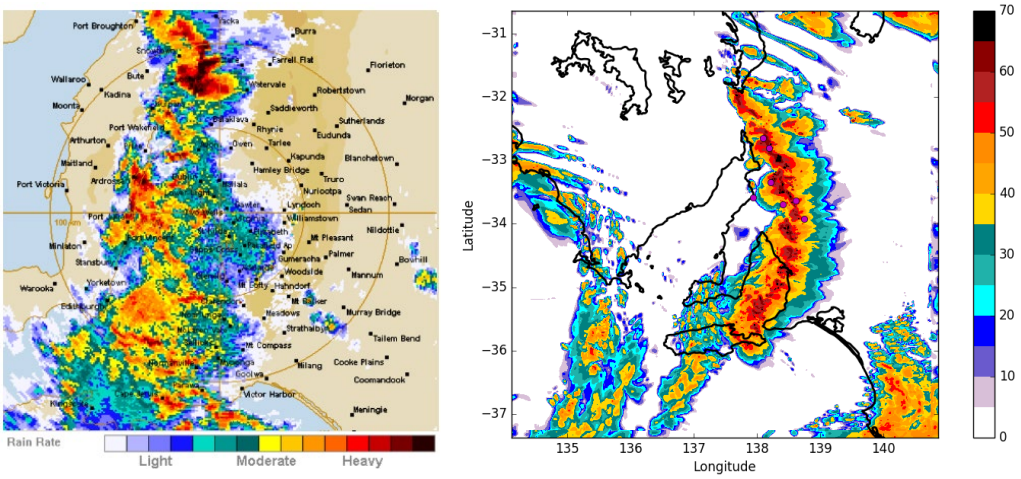

Figure 2: (Left) Observed radar reflectivity and (right) simulated radar reflectivity at 0600 UTC 28 September 2016. The magenta dots in the right panel are the observed locations of the tornadoes.

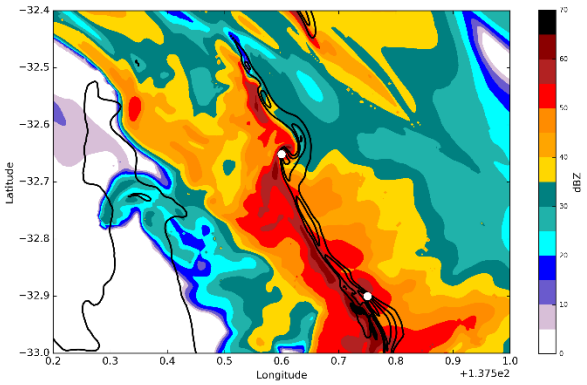

Figure 3: 0600 UTC 28 September 2016 simulated radar reflectivity (dBZ) at 2 km height for the 400-m simulation. The white dots are the observed locations of the tornadoes and the black box denotes the area shown in Fig. 4.

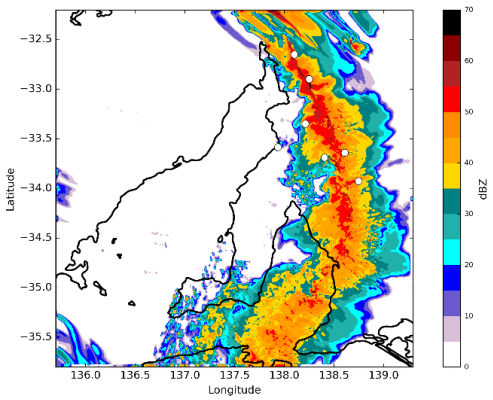

Figure 3: As for Fig. 3, only for area denoted by the black box in Fig. 3.

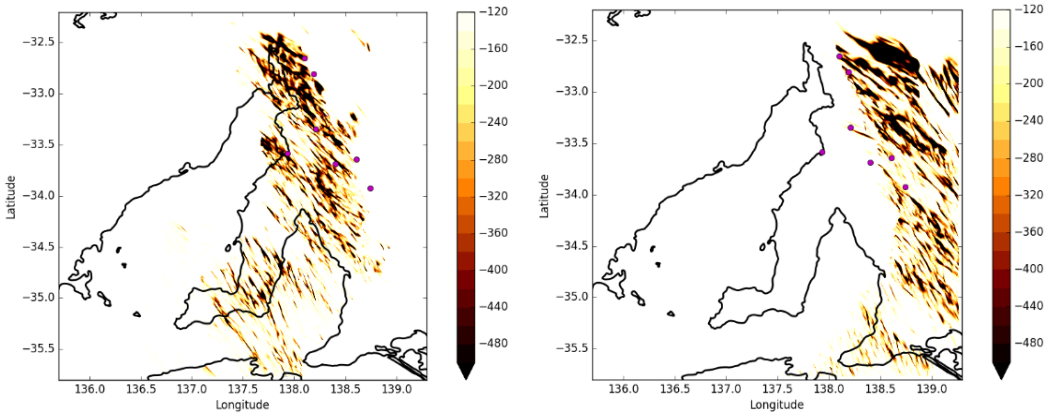

Figure 4: Hourly minimum updraft helicity (UH, $m^2\ s^{-2}$) for the period (left) 0500-0600 UTC 28 September 2016 and (right) 0600-0700 UTC 28 September 2016. The magenta dots denote the approximate location of observed tornadoes.

Figure 3 shows simulated reflectivity from the 400-m simulation, where the northern cells (black box in Fig. 3) are stronger and better defined than the southern part of the convective system, indicated by differences in the simulated reflectivity. A close-up view of the simulated reflectivity and vertical velocity (Fig. 4) in the northern part of the system (black box in Fig. 3) reveals a hook-echo feature and a curved updraft that coincide with the location of one of the reported tornadoes (northernmost white dot in Fig. 4). The hook echo indicates the presence of a mesocyclone (Davies-Jones 2015) at this location. The reported tornado is estimated to have started at approximately 0615 UTC, 28 September 2016 (Bureau of Meteorology 2016; Sgarbossa et al. 2018), which is about 15 min later than in the simulation. Therefore, the mesocyclone and features that indicate the possibility of a tornado are well captured with the 400-m simulation.

Based on (Kain et al. 2008), a model diagnostic field (updraft helicity) is used to investigate the ability of the model to identify the potential for supercell thunderstorms, within which tornadoes may form.

Updraft helicity (UH) is the product of vertical vorticity and vertical velocity, integrated vertically from 2 km to 5 km:

$$\boldsymbol{UH = \int_{2km}^{5km} w\left(\frac{\partial v}{\partial x} - \frac{\partial u}{\partial y}\right) dz},$$

where w is vertical velocity ($m\ s^{-1}$), $\left(\frac{\partial v}{\partial x} - \frac{\partial u}{\partial y}\right)$ is vertical vorticity (s^{-1}) and z is height (m). Relevant values of UH are negative in the Southern Hemisphere (SH). While UH can be computed as an instantaneous value at a single model output time, (Kain et al. 2010) developed hourly maximum UH that tracks the maximum (minimum in the SH) value of the diagnostic at every grid point at any model time step within the previous hour (e.g., Clark et al. 2012, 2013; Sobash et al. 2016). Here, UH is computed in this way as an output diagnostic in the Met Office UM model.

Figure 5 shows hourly minimum UH for the period between 0500-0600 UTC and 0600-0700 UTC 28 September 2016, which coincides with the time period of the reported tornadoes (Bureau of Meteorology 2016). It shows elongated swaths of hourly minimum UH exceeding -120 $m^2 s^{-2}$ and reaching values < -400 $m^2 s^{-2}$ in close proximity to the observed tornadoes (magenta dots in Fig. 5). A long and coherent, vortex-like swath of hourly minimum UH < -500 $m^2 s^{-2}$ coincides with the location of the northernmost observed tornado, where the mesocyclone was identified in simulated reflectivity and vertical velocity (cf. Fig. 4). This indicates that the use of UH as a diagnostic field would have provided useful guidance for identifying the potential for tornado formation in this case. Another parameter that is worth investigating as a tornado proxy alongside UH is the Okubo-Weiss (OW) parameter, defined as

$$OW = \zeta^2 - (E^2 + F^2) = \left(\frac{\partial v}{\partial x} - \frac{\partial u}{\partial y}\right)^2 - \left\{\left(\frac{\partial u}{\partial x} - \frac{\partial v}{\partial y}\right)^2 + \left(\frac{\partial v}{\partial x} + \frac{\partial u}{\partial y}\right)^2\right\},$$

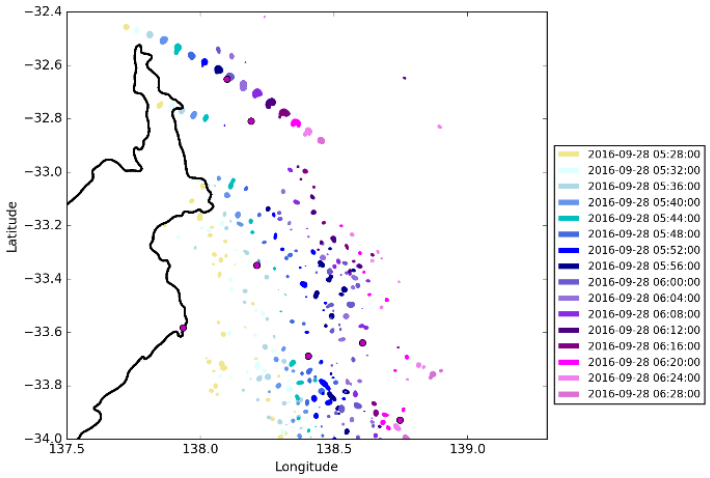

Figure 5: The Okubo-Weiss parameter (OW; positive values only), calculated as a 1 km-4 km layer average for the time interval between 0528 UTC and 0628 UTC 28 September 2016. The magenta dots denote the approximate location of observed tornadoes.

where ζ is the vertical vorticity, E is the stretching deformation, and F is the shearing deformation (Okubo 1970; Weiss 1991; Markowski et al. 2011). The OW parameter highlights flow regions where rotation dominates over strain, and therefore can be used to identify rotation (or vortices) associated with tornadic storms (e.g., Markowski et al. 2011; Coffer & Parker 2016).

Figure Figure 5 shows the OW parameter calculated as per the above equation, using layer averaging between 1 km and 4 km at 4-minute intervals during the time interval between 0528 UTC and 0628 UTC 28 September 2016. It shows a coherent track of positive OW parameter that coincides with the location of the northernmost reported tornado, thus clearly identifying the mesocyclone in this simulation. This analysis shows that the OW parameter identifies the rotation associated with the mesocyclone in these simulated storms and gives a clear indication of a tornado path. This suggests it can be used as an additional diagnostic alongside UH to assess tornado potential, thus potentially reducing false alarms.

b) Ensemble simulations

shows the simulated radar reflectivity for each ensemble member and should be compared to
Figure 2. The variation in the mode of convection is immediately apparent. While members 1, 2 and 5 display a QLCS structure quite similar to the deterministic forecast, member 0 is weaker to the north, member 4 is weaker throughout, member 3 has independent cells of convection rather than a QLCS.

The results from the convective diagnostic tools from these simulations possess a similarly wide range, although for reasons of space we show only the UH. Hourly minimum fields of UH for the six ensemble members are shown in Figure 7, with members 1 and 2 again being the most like the deterministic simulation. The four individual convective cells in member 3 each possess a strong band of intense UH, suggesting that these four cells are individual supercells, in contrast to the QLCS structure of members 1 and 2. The weaker UH in the remaining members is indicative of less

The analysis presented in the previous section is based on the deterministic, high-resolution simulations that enable the study of the dynamics and properties of tornadic storms, as well as highlighting how diagnostics such as UH and the OW parameter could be used as severe storm surrogates.

However, they do not provide information on the uncertainty associated with the timing, location and intensity of the tornadic storms or tornado pathlengths (e.g., Hanley, Barrett & Lean 2016; Snook, Xue & Jung 2019). Therefore, convection-allowing (i.e. grid lengths on the order of O(1km)) ensemble simulations are necessary to overcome these issues and to improve forecasting of severe storms and associated hazards, as tornado-resolving ensemble simulations are not very practical due to extreme computational costs involved (e.g., Zhang et al. 2015; Sobash, Schwartz, et al. 2016; Snook, Xue & Jung 2019).

The ensemble simulations showed some differences to the deterministic simulation described above. The most important of these is about a half-hour difference in timing of the event, likely due to the use of a different global initial condition.

favorable, but not impossible, conditions for tornadogenesis.

Summary

The deterministic simulation, and two of the six ensemble members, produced simulated radar reflectivity plots whose structure, orientation, timing and intensity were in close agreement with the observations. In the remaining ensemble members, the convection was either weaker, or displayed a different structure, to that observed.

In the deterministic simulation, a strong mesovortex embedded in the main rainband closely agreed in position and timing with one of the observed tornadoes. Numerous diagnostics of mesovortex formation were examined, of which two demonstrated strong utility: the updraft helicity and the Okubo-Weiss parameter.

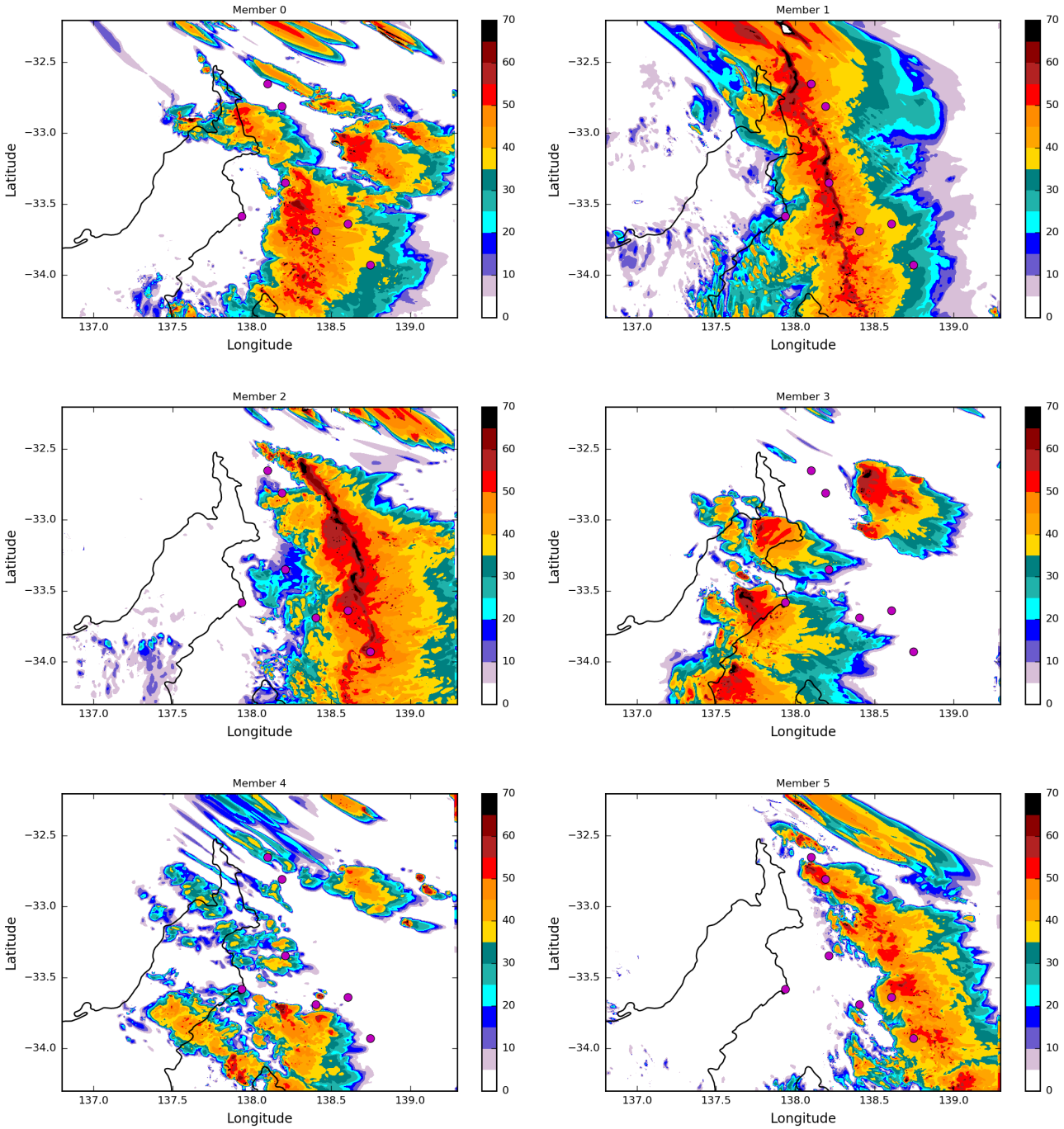

Figure 6: Snapshots of simulated radar reflectivity from the ensemble simulation.

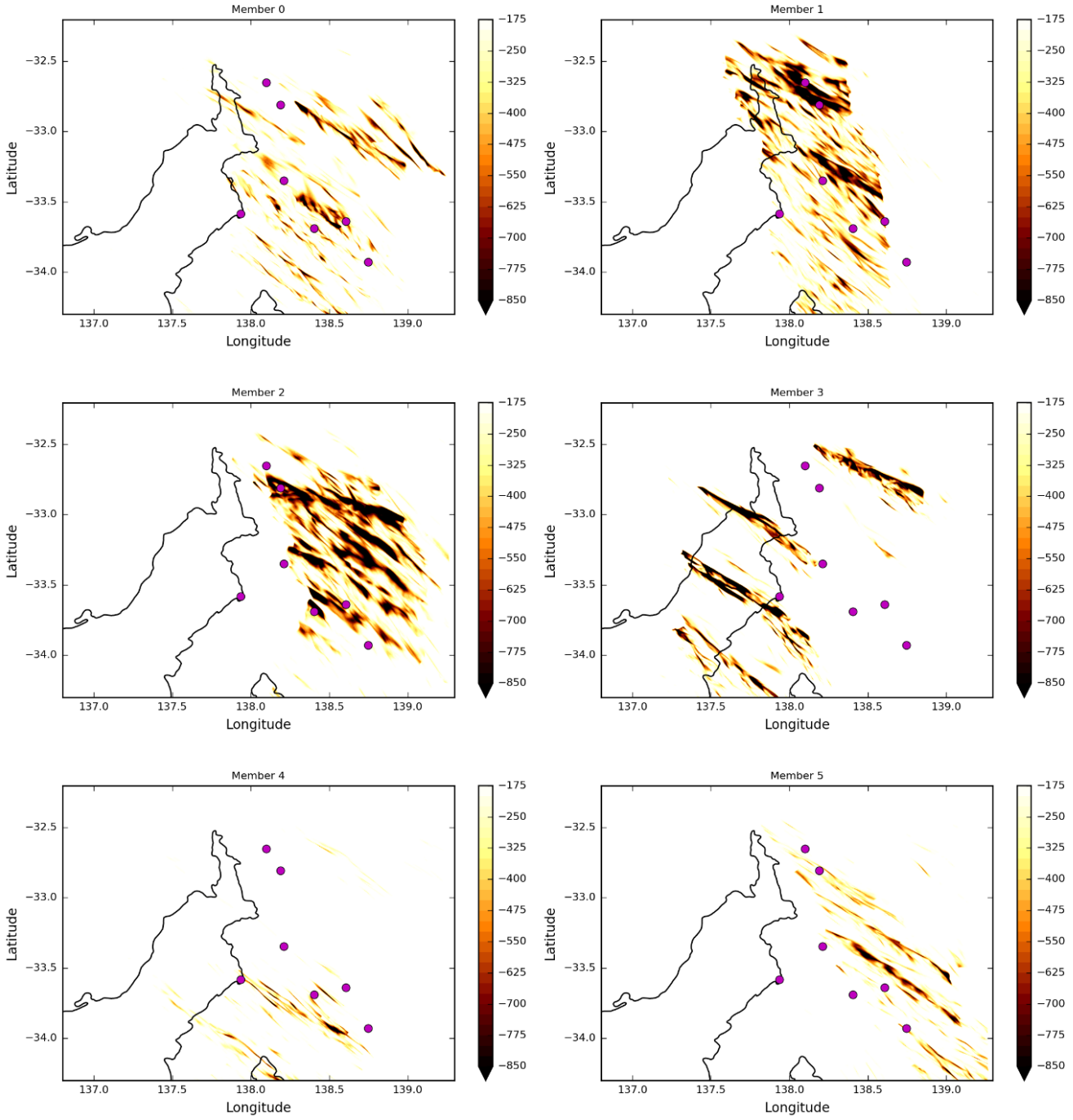

Figure 7: Hourly minimum updraft helicity (UH, $m^2\ s^{-2}$) for the 6 ensemble members.

The ensemble simulations highlight the uncertainty associated with timing, location and intensity of the convective systems that spawned the tornadoes. While each of the members indicated some potential for tornado formation, this potential varied in magnitude, timing and location between the members. It may not be appropriate to assign a numerical probability to tornado formation in this case, since the ensemble has not been calibrated for this purpose. Nevertheless, such an ensemble would have strongly supported a forecast of a high risk of tornado formation.

This ensemble simulation also presents a good example of an important advantage of ensembles over deterministic simulations. The control member of the ensemble (i.e. the unperturbed member 0) provided a more modest indication of tornadoes, especially to the north of the region of interest, as did two of the others. If any of these had been the sole deterministic member available, the forecasters would have not received as strong an indication of the potential for tornadoes. A single deterministic forecast can be regarded as a random choice from the set of all possible ensemble members. Although in this case the deterministic forecast happened to strongly indicate tornado risk, it could well have been weaker. The most extreme forms of severe weather are, almost by definition, rare events. Thus, the use of an ensemble reduces the chances the numerical guidance will unluckily miss the true magnitude of the event.

References

Bowler, NE, Arribas, A, Mylne, KR, Robertson, KB & Beare, SE 2008, 'The MOGREPS short-range ensemble prediction system', *Quarterly Journal of the Royal Meteorological Society*, vol. 134, no. 632, pp. 703–722.

Bryan, GH, Wyngaard, JC & Fritsch, JM 2003, 'Resolution requirements for the simulation of deep moist convection', *Monthly Weather Review*, vol. 131, no. 10, pp. 2394–2416.

Bureau of Meteorology 2016, Severe thunderstorm and tornado outbreak South Australia 28 September 2016.

Bush, M, Allen, T, Bain, C, Boutle, I, Edwards, J, Finnenkoetter, A, Franklin, C, Hanley, K, Lean, H, Lock, A, Manners, J, Mittermaier, M, Morcrette, C, North, R, Petch, J, Short, C, Vosper, S, Walters, D, Webster, S, Weeks, M, Wilkinson, J, Wood, N & Zerroukat, M 2019, 'The first Met Office Unified Model/JULES Regional Atmosphere and Land configuration, RAL1', *Geoscientific Model Development Discussions*, vol. in review, no. June, pp. 1–47.

Clark, AJ, Gao, J, Marsh, PT, Smith, T, Kain, JS, Correia, J, Xue, M & Kong, F 2013, 'Tornado Pathlength Forecasts from 2010 to 2011 Using Ensemble Updraft Helicity', *Weather and Forecasting*, vol. 28, no. 2, pp. 387–407.

Clark, AJ, Kain, JS, Marsh, PT, Correia, J, Xue, M & Kong, F 2012, 'Forecasting Tornado Pathlengths Using a Three-Dimensional Object Identification Algorithm Applied to Convection-Allowing Forecasts', *Weather and Forecasting*, vol. 27, no. 5, pp. 1090–1113.

Coffer, BE & Parker, MD 2016, 'Simulated Supercells in Nontornadic and Tornadic VORTEX2 Environments', *Monthly Weather Review*, vol. 145, no. 1, pp. 149–180.

Davies-Jones, R 2015, 'A review of supercell and tornado dynamics', *Atmospheric Research*, vol. 158–159, pp. 274–291.

Hanley, KE, Barrett, AI & Lean, HW 2016, 'Simulating the 20 May 2013 Moore, Oklahoma tornado with a 100-metre grid-length NWP model', *Atmospheric Science Letters*, vol. 17, no. 8, pp. 453–461.

Kain, JS, Dembek, SR, Weiss, SJ, Case, JL, Levit, JJ & Sobash, RA 2010, 'Extracting Unique Information from High-Resolution Forecast Models: Monitoring Selected Fields and Phenomena Every Time Step', *Weather and Forecasting*, vol. 25, no. 5, pp. 1536–1542.

Kain, JS, Weiss, SJ, Bright, DR, Baldwin, ME, Levit, JJ, Carbin, GW, Schwartz, CS, Weisman, ML, Droegemeier, KK, Weber, D & Thomas, KW 2008, 'Some practical considerations regarding horizontal resolution in the first generation of operational convection-allowing NWP', *Weather and Forecasting*, vol. 23, pp. 931–952.

Markowski, P, Majcen, M, Richardson, Y, Marquis, J & Wurman, J 2011, 'Characteristics of the wind field in a trio of nontornadic low-level mesocyclones observed by the Doppler On Wheels radars', *E-Journal of Severe Storms Meteorology*, vol. 6, no. 3, pp. 1–48.

Okubo, A 1970, 'Horizontal dispersion of floatable particles in the vicinity of velocity singularities such as convergences', *Deep Sea Research and Oceanographic Abstracts*, vol. 17, no. 3, pp. 445–454.

Puri, K, Dietachmayer, G, Steinle, P, Dix, M, Rikus, L, Logan, L, Naughton, M, Tingwell, C, Xiao, Y, Barras, V, Bermous, I, Bowen, R, Deschamps, L, Franklin, C, Fraser, J, Glowacki, T, Harris, B, Lee, J, Le, T, Roff, G, Sulaiman, A, Sims, H, Sun, X, Sun, Z, Zhu, H, Chattopadhyay, M & Engel, C 2013, 'Implementation of the initial ACCESS numerical weather prediction system', *Australian Meteorological and Oceanographic Journal*, vol. 63, no. 2, pp. 265–284.

Sgarbossa, D, Fischer, J, Bass, M & Taylor, J 2018, 'The end-to-end convective hazard risk forecast process developed by the Australian Extreme Weather Desk for the South Australian 28 September 2016 tornado outbreak', in 29th Conf. on Severe Local Storms, Stowe, VT, Amer. Meteor. Soc.

Snook, N, Xue, M & Jung, Y 2019, 'Tornado-Resolving Ensemble and Probabilistic Predictions of the 20 May 2013 Newcastle–Moore EF5 Tornado', *Monthly Weather Review*, vol. 147, no. 4, pp. 1215–1235.

Sobash, RA, Romine, GS, Schwartz, CS, Gagne, DJ & Weisman, ML 2016, 'Explicit Forecasts of Low-Level Rotation from Convection-Allowing Models for Next-Day Tornado Prediction', *Weather and Forecasting*, vol. 31, no. 5, pp. 1591–1614.

Sobash, RA, Schwartz, CS, Romine, GS, Fossell, KR & Weisman, ML 2016, 'Severe Weather Prediction Using Storm Surrogates from an Ensemble Forecasting System', *Weather and Forecasting*, vol. 31, no. 1, pp. 255–271.

Weisman, ML & Trapp, RJ 2003, 'Low-level mesovortices within squall lines and bow echoes. Part I: Overview and dependence on environmental shear', *Monthly Weather Review*, vol. 131, no. 11, pp. 2779–2803.

Weiss, J 1991, 'The dynamics of enstrophy transfer in two-dimensional hydrodynamics', Physica D: Nonlinear Phenomena, vol. 48, no. 2, pp. 273–294.

Zhang, Y, Zhang, F, Stensrud, DJ & Meng, Z 2015, 'Practical Predictability of the 20 May 2013 Tornadic Thunderstorm Event in Oklahoma: Sensitivity to Synoptic Timing and Topographical Influence', *Monthly Weather Review*, vol. 143, no. 8, pp. 2973–2997.